Numerical Analysis of Rarefied Propellant Flow within a Vacuum Chamber and Comparison to Experimental Data

By Keita NISHII,[1)] Akira KAKAMI,[1)] Tsubasa ITO,[2)] and Yoshinori NAKAYAMA[2)]

[1)]*Department of Aeronautics and Astronautics, Tokyo Metropolitan University, Tokyo, Japan*
[2)]*Department of Aerospace Engineering, National Defense Academy, Kanagawa, Japan*

A GPU-accelerated DSMC solver with adaptive mesh refinement was developed and applied to simulate rarefied xenon gas flows in a vacuum chamber. The model was constructed to accurately reproduce the boundary conditions at the gas tube exit and to enable direct comparison with experiments using rarefied gas measurement devices. Simulations were performed for various wall accommodation coefficients and gas injection angles. Although absolute values differed between simulation and experiment, which was mainly due to probe uncertainties and simplified reflection models, the normalized distributions showed good agreement. The flow reflected at the wall changes with the accommodation coefficient, and the difference between the simulation and experimental values was minimized when the accommodation coefficient was set to 0.9. These results indicate that a combined experimental and numerical approach to determining the wall accommodation coefficient is valuable for future vacuum chamber environment simulations. The findings also highlight several areas for improvement that will enable more faithful comparison between experiments and simulations.

Key Words: Space propulsion, Facility effect, Electric propulsion, Rarefied gas flow, DSMC method

1. Introduction

Electric propulsion (EP) systems, such as ion engines and Hall thrusters, have become key technologies for space exploration missions and satellite station-keeping, owing to their high specific impulse and efficient propellant utilization. The performance characterization and ground qualification of such thrusters rely heavily on ground-based vacuum testing. However, the test environment cannot perfectly replicate the conditions of space. Factors such as elevated background pressure, electrical connectivity to the vacuum chamber, and contamination due to back-sputtering can significantly affect thruster performance and lifetime predictions.[1,2)] This problem, known as the facility effect, has become increasingly recognized as a major concern in recent years, particularly as EP systems have grown larger in scale.

The primary cause of facility effects is the interaction between the propellant plume and the chamber walls. In a vacuum chamber, propellant gas expelled from the thruster undergoes multiple collisions with the chamber walls before being exhausted, resulting in a background pressure that is three orders of magnitude or more higher than that in space. The probability and nature of wall reflection strongly depend on factors such as surface material, temperature, roughness, and the energy of the incident particles. As a result, accurately predicting the distribution of neutral particles inside the chamber is challenging, and numerical methods have been employed to predict the gas distribution inside a vacuum chamber. Because the vacuum chamber environment is extremely rarefied, conventional continuum-based computational fluid dynamics (CFD) methods are not applicable. Instead, the direct simulation Monte Carlo (DSMC) method has been used as the standard approach for vacuum chamber analysis.[3,4)]

One difficulty in modeling a vacuum chamber using the DSMC method is the treatment of gas-surface interactions. The reflection of gas molecules from solid surfaces is often characterized by the accommodation coefficient, which quantifies the extent to which molecules exchange energy and momentum with the wall. In practice, the accommodation coefficient is influenced by gas species, wall material, surface condition, temperature, and the incident angle of the particles.[5–7)] The lack of comprehensive empirical data for all relevant combinations leads to considerable uncertainty in the choice of boundary conditions for simulations. Therefore, experimental validation is essential for assessing the realism of numerical models.

Recent work by Nakayama et al.[8,9)] has led to the development and validation of S-type and P-type rarefied gas measurement devices for visualizing neutral particle flows inside vacuum chambers. Experimental measurements using these probes have yielded new data not only on the spatial distribution of neutral propellant within the chamber but also on static and dynamic pressures. Furthermore, an experimental system was constructed to estimate the wall accommodation coefficient by injecting gas toward the target wall and measuring the reflected gas.[10,11)] While these probes alone cannot directly determine the wall accommodation coefficient or the pumping efficiency, they serve as valuable tools for validating numerical simulations.

In this study, we simulate the experimental setup of the rarefied flow measurement system using the DSMC method. To efficiently handle the expanding flow from the gas tube, which is the focus of this study, under various parameter settings, we have developed a GPU-accelerated solver employing adaptive mesh refinement. By performing simulations with this solver and comparing the results with experiments, we aim to mutually evaluate the validity of both the experimental device and the simulation tool. In addition, this study clarifies the current limitations of wall accommodation coefficient estimation and outlines future directions for improving accuracy.

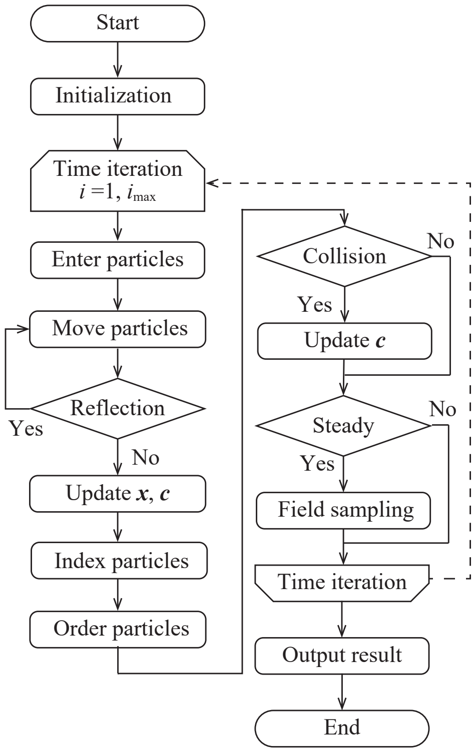

Fig. 1. Flow chart of the DSMC solver developed in this study.

2. Numerical Method

2.1. Direct Simulation Monte Carlo Approach

The direct simulation Monte Carlo (DSMC) method[12] is widely employed to model rarefied gas flows encountered in vacuum chambers, particularly in the context of electric propulsion testing where the Knudsen number is large. In this study, we utilized an in-house DSMC code, which was originally validated in Ref.[13] and ported to CUDA, enabling massive parallelization. We used a two-dimensional axisymmetric code for the gas tube simulation and a fully three-dimensional Cartesian code for the gas reflection geometry.

Our DSMC workflow is illustrated in Fig. 1. During the time-marching loop, no particle data are exchanged between the GPU and CPU, which provides a substantial speed-up. The computational mesh was generated at the initialization step based on adaptive mesh refinement (AMR) combined with an octree method.[14–16]

The treatment of gas-surface interactions is of particular importance for analyzing facility effects. Here, the Maxwell boundary condition is applied to all chamber walls: a fraction α of incoming particles undergo diffuse (thermal) reflection, acquiring a new velocity sampled from the wall temperature, while the remainder $(1 - \alpha)$ are specularly reflected. The accommodation coefficient α was systematically varied (from 0.0 to 1.0).

2.2. Simulation Geometries

The entire numerical setup, schematized in Fig. 2, closely follows the experimental system described in Ref.[9] The main features include a narrow gas injection tube (inner diameter 1.755 mm, length 50 mm) feeding xenon into a test volume, a target wall for reflection studies, and a probe region for flux measurement.

We first simulated the flow inside the gas tube to obtain the physical quantities at its exit. Figure 3 shows the simulation conditions within the gas tube. The inlet boundary condition was set to a pressure that reproduces the experimentally specified xenon mass flow rate of 0.67 mg/s. In this simulation, the radial direction was discretized into 100 cells, and for each cell, the temperature, velocity, and flux at the tube exit (downstream boundary) were sampled in the x-, y-, and z-directions.

Based on the results at the gas tube exit, these quantities were then used as boundary conditions for the subsequent simulation of the entire wall reflection measurement apparatus. Gas is injected from the gas tube toward the target wall, as shown in Fig. 2. Only half of the experimental region was simulated, with the $z = 0$ m plane treated as a symmetry boundary. All outer boundaries except for the wall allow free outflow of gas, and a prescribed pressure was applied to introduce background gas flow in the reverse direction. Numerical probe measurements were performed along a semicircle with a radius of 165 mm centered on the point where the gas tube faces the target wall. In this setup, the physical device structure is not explicitly modeled; instead, local flow properties are evaluated by directly sampling the simulation particles.

2.3. Rarefied Flow Measurement Devices and Numerical Sampling

It is essential to calculate quantities that are directly comparable to those measured by rarefied flow detectors in experiments. This study considered two types of rarefied gas measurement devices: S-type and P-type.[9] These devices are designed to evaluate either the force or pressure at a specific location inside the vacuum chamber.

2.3.1. Force Measurement Probe: S-type

The S-type probe measures the force exerted on its surface by the incident gas molecules. The schematic of the measurement probe is illustrated in Fig. 4. The system detects light emitted from an optical fiber using a photodetector, and measures the displacement of the fiber caused by the force resulting from the pressure difference between the front-side and back-side rarefied gas acting on the fiber. Details of this measurement device can be found in Ref.[17]

Assuming that the rarefied flow uniformly impinges on the fiber with a length of L and a diameter of d, the rarefied gas dynamic pressure $p_{\rm f}$ detected by the fiber can be expressed as:

$$p_f = \frac{F_{\rm f}}{C_{\rm d} d L} \tag{1}$$

where $F_{\rm f}$ is the force detected by the S-type probe and $C_{\rm d}$ is the drag coefficient. If the incident particles undergo completely diffuse reflection on the cylindrical fiber surface, $C_{\rm d}$ is taken to be 1.785.

In the DSMC simulation, this device is not modeled explicitly. Instead, the rarefied dynamic pressure p_d at the probe location is obtained by directly sampling particles. Below, we present expressions for p_d using the velocity distribution function $f(v)$ and in terms of discrete computational particle sam-

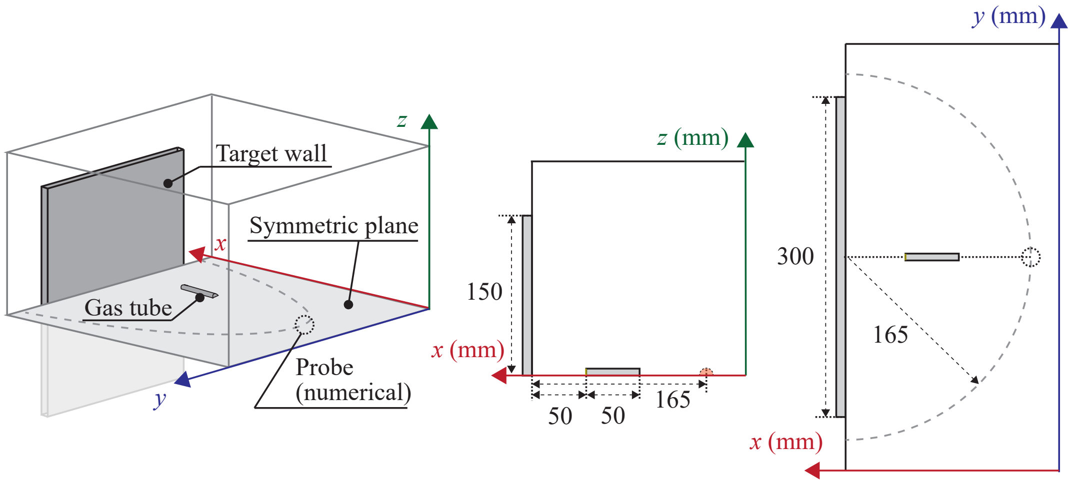

Fig. 2. Simulation geometry for the rarefied gas flow detector experiment.

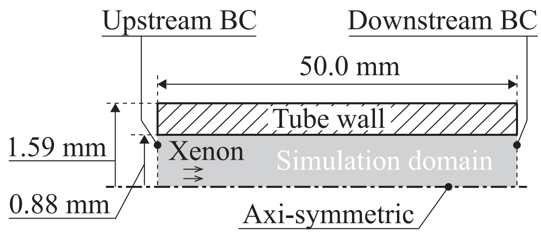

Fig. 3. Gas tube simulation geometry.

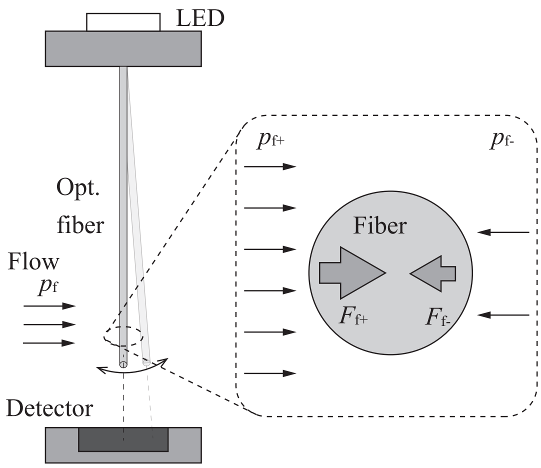

Fig. 4. Schematic of the S-type rarefied gas measurement device.

ples:

$$p_d = \int_0^{\infty} mn\, v_r^2\, f(v)\, dv - \int_{-\infty}^{0} mn\, v_r^2\, f(v)\, dv \tag{2}$$

$$= \frac{f_{\mathrm{num}}}{A_{\mathrm{smp}}\, i_{\mathrm{smp}}\, \Delta t} \left(\sum_{\substack{i=1 \\ v_{r,i}>0}}^{N_{\mathrm{smp},+}} m\, v_{r,i} - \sum_{\substack{i=1 \\ v_{r,i}<0}}^{N_{\mathrm{smp},-}} m\, v_{r,i} \right) \tag{3}$$

Here, n is the number density of particles, m is the molecular mass, and v_r is the sample velocity component defined as positive in the direction away from the wall. For discrete sampling, f_{num} is the number of real particles represented by one simulation particle, A_{smp} is the sampling surface area, i_{smp} is the number of sampling steps in the simulation, Δt is the time per step, and N_{smp} is the total number of sampled simulation particles. By introducing a coefficient β that characterizes the momentum transferred in the reverse direction due to wall reflection, the

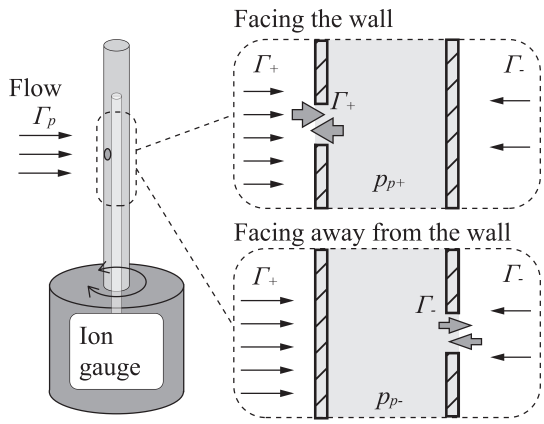

Fig. 5. Schematic of the P-type rarefied gas measurement device.

dynamic pressure on the fiber can be expressed as:

$$p_f = \beta \cdot p_d. \tag{4}$$

Here, $\beta = 1$ corresponds to the case where the particles stick to the surface or are reflected from a perpendicular wall, while $\beta = 2$ corresponds to perfect specular reflection from a perpendicular wall. Therefore, the range of β is considered between 1 and 2.

2.3.2. Pressure Measurement Probe: P-type

The P-type probe consists of an ion gauge connected to a cavity with a single orifice. By adjusting the angle and position of the orifice, the probe outputs the pressure measured by the ion gauge, as illustrated in Fig. 5. Although the geometry of this probe differs from the P-type described in Ref.,[10] the principle remains the same.

After a sufficient period, the particle flux Γ through the orifice reaches equilibrium between inflow and outflow. Assuming that the particle density and temperature inside the probe are uniform, the incoming flux can be calculated from the measured pressure p_{p} and device temperature T_{p} as follows:

$$\Gamma = \frac{p_{\mathrm{p}}}{\sqrt{2\pi m k_{\mathrm{B}} T_{\mathrm{p}}}} \tag{5}$$

Therefore, by measuring the pressures $p_{\mathrm{p},+}$ when the orifice faces the reflecting surface and $p_{\mathrm{p},-}$ when it faces the opposite direction, the net particle flux Γ_p passing through the measurement point can be obtained as follows:

$$\Gamma_p = \frac{p_{p,+} - p_{p,-}}{\sqrt{2\pi m k_B T_p}} \tag{6}$$

In the DSMC simulation, the particle flux can be obtained as follows:

$$\Gamma = \int_{-\infty}^{\infty} mn\, v_r\, f(v)\, dv \tag{7}$$

$$= \frac{f_{num}\left(N_{smp,+} - N_{smp,-}\right)}{A_{smp}\, i_{smp}\, \Delta t} \tag{8}$$

where the notation is consistent with that used in Eq. (3).

3. Results and Discussion

3.1. Simulation inside Gas Tube

It is common to assume a uniform flux and velocity (Mach number of one) in the radial direction for gas jet injection from the tube into a vacuum. However, this assumption can introduce significant errors when more accurate predictions are required. Therefore, before simulating the entire reflection region (Fig. 2), we performed calculations inside the gas tube (Fig. 3) to obtain precise gas injection boundary conditions. The Knudsen number at the tube inlet was approximately 0.01, while at the outlet it was about 0.1. This means that the outlet cannot be accurately treated as a continuum flow, and thus it was appropriate to use DSMC for the calculation.

Figure 6 shows, for each of the 100 cells in the radial direction, the axial particle flux, the average velocities in the x, y, and z directions, and the temperatures estimated from the Maxwell-Boltzmann distribution. As R increases, both the density and the axial (x-direction) velocity decrease, leading to a reduction in flux. The increase in y-direction velocity near the tube wall indicates greater divergence of the gas in those regions. The temperature profiles reveal non-equilibrium between the x direction and the y/z directions. Based on the flux profile shown in the figure, the inflow particle number at the boundary was determined. The states of particles injected from the gas tube exit were sampled using a Maxwell-Boltzmann velocity distribution constructed from the local mean velocity and temperature, applying the acceptance-rejection method.

3.2. Simulation of Xenon Flow in the Experimental Geometry

The gas injection boundary conditions obtained in Section 3.1 were applied to the geometry shown in Fig. 2 to simulate the wall-reflected flow. The background pressure was set to 4.0 mPa.[10] As simulation parameters, the gas injection angle was set to either 0 degrees or 45 degrees, and the wall accommodation coefficient α was varied among 0, 0.8, 0.9, and 1.0.

Figure 7 presents the calculated number density distributions of gas molecules in the $z = 0$ m plane (probe scanning plane). Here, as representative cases, results are shown for gas injection angles of 0 degrees and 45 degrees, each with $\alpha = 0$ (specular reflection) and $\alpha = 1$ (diffuse reflection). The spreading of gas from the tube and the diffusion after wall reflection can be observed. It is evident that the high-density region behind the gas tube is broader for $\alpha = 1$ (diffuse reflection) than for $\alpha = 0$ (specular reflection).

3.3. Comparison with Experimental Measurements

In this section, we compare the numerical simulation results with measurements obtained using two types of probes.

3.3.1. Momentum Flux (S-type)

We first focus on the dynamic pressure values measured by the S-type probe (Fig. 4). The experimental data are taken from Ref.[10] For simplicity, the parameter β in Eq. (4) is set to 1.0 in this analysis. Figure 8 shows the results for three different gas injection angles: (a) $\theta = 0°$, (b) 45°, and (c) −45°. In the case of −45°, the experimental data were obtained separately for positive and negative angles, but for the numerical simulation, the result at 45° was mirrored and used for −45°.

The simulation results indicate that as the accommodation coefficient α increases, the peak momentum flux at around 20° decreases, while the values near 0° and above 60° increase. For $\alpha = 1$ (diffuse reflection), the distribution becomes nearly uniform within the range of −30° to 30°.

Except for the extreme case of $\alpha = 0$, all experimental values were lower than the corresponding simulation results for every reflection angle. A major reason for this is that, as shown in Eq. (1), the S-type probe experiment assumes that the fiber experiences a uniform force in the z-direction over its entire length, whereas the present numerical sampling only considers the $z = 0$ m plane, where the force is expected to be highest.

3.3.2. Particle Number Flux (P-type)

Next, we compare the experimental and simulated particle fluxes using results from the P-type probe. The experimental data are taken from Ref.[11] Figure 9 presents the results for three gas injection angles: (a) $\theta = 0°$, (b) 45°, and (c) −45°. The trends with respect to the accommodation coefficient in the simulation are similar to those observed in the S-type comparison shown in Fig. 8.

On the other hand, in this comparison, the experimental values are significantly larger than the simulation results. The analysis assumes that the pressure inside the P-type probe is uniform; however, the actual pressure at the measurement point is always higher than that near the orifice. By numerically analyzing the internal flow within the P-type probe, it should be possible to quantitatively assess this discrepancy. Furthermore, the uncertainty of an ionization gauge is relatively large (greater than 10%). Since the measurements were carried out under relatively high background pressure conditions (9.2 mPa), the pressure difference between $p_{s,+}$ and $p_{s,-}$ was small, which likely contributed to additional uncertainty in the measurements.

3.3.3. Normalized Values

Up to this point, we have quantitatively compared the values obtained from experiments and numerical simulations; however, due to the assumptions made during analysis and uncertainties in the measurement devices, a direct comparison was not possible. To eliminate uncertainties in absolute sensitivity and facilitate meaningful comparison, both experimental and simulation results were normalized by their respective mean values near the measurement point. This approach allows for robust trend analysis, even when systematic measurement errors are present. In fact, as demonstrated in Ref.,[11] the S-type and P-type probe values exhibit similar trends when normalized by their respective mean values. Therefore, in this study, we compare the experimental and simulated results using nor-

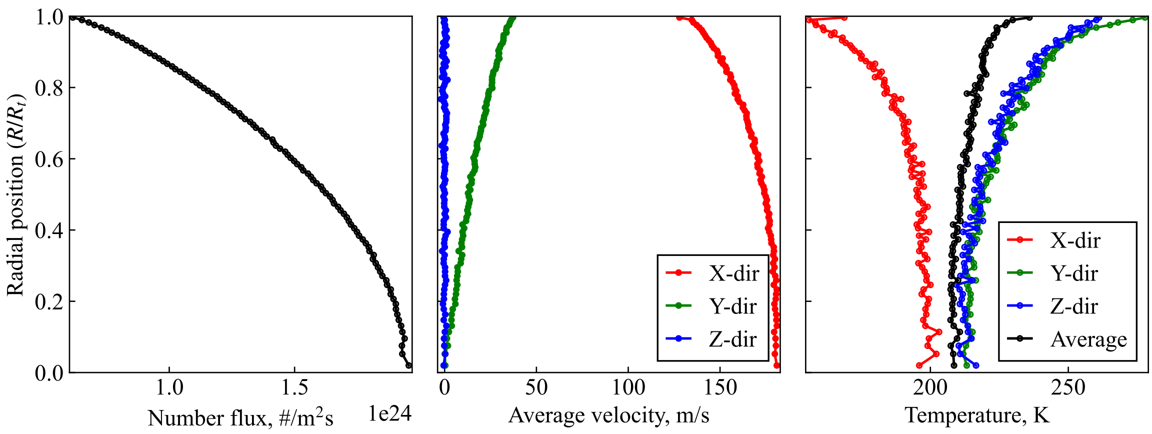

Fig. 6. Sampled field values at the gas-tube exit.

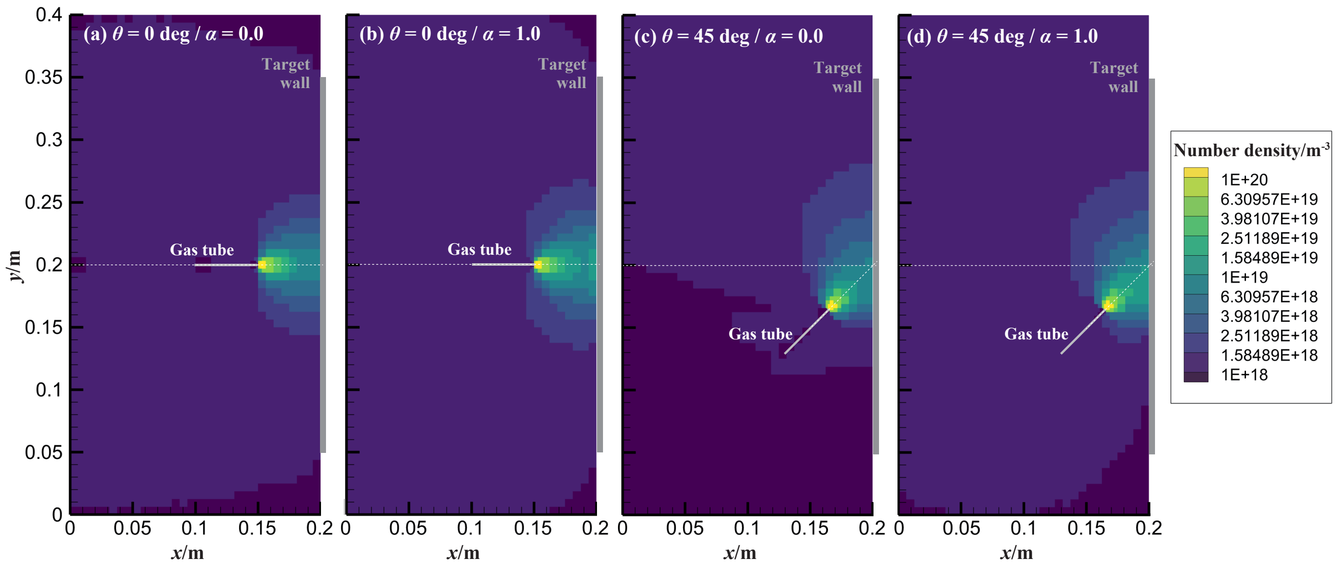

Fig. 7. Number density at z = 0.0 m plane for four cases: (a) $\theta = 0°$, $\alpha = 0.0$; (b) $\theta = 0°$, $\alpha = 1.0$; (c) $\theta = 45°$, $\alpha = 0.0$; and (d) $\theta = 45°$, $\alpha = 1.0$, where θ is the gas incident angle and α is the accommodation coefficient for the Maxwell reflection model.

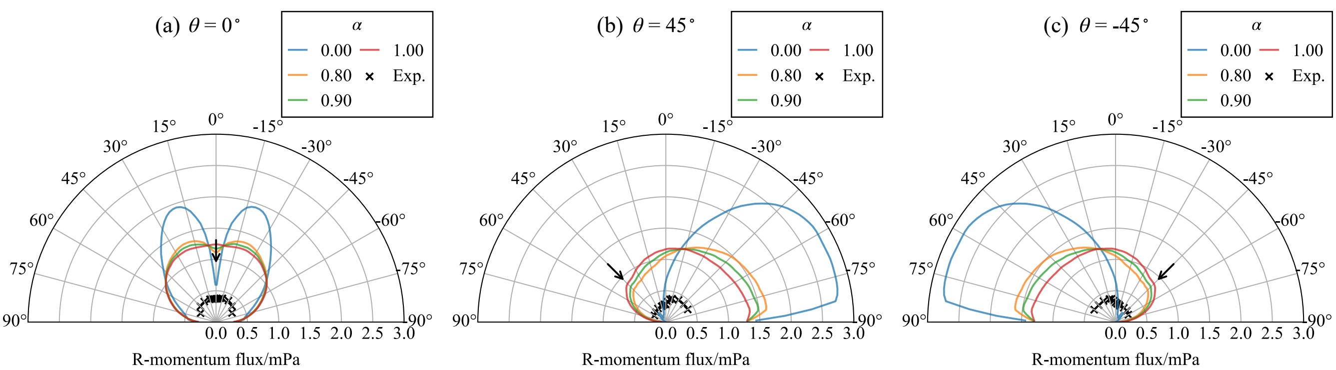

Fig. 8. Simulation results of the momentum flux (with $\beta = 1$) in the probe radial direction for different values of the accommodation coefficient α with (a) $\theta = 0°$, (b) 45°, and (c) −45°. Cross plots indicate experimental values.[10)]

malized values.

Figure 10 shows, for (a) $\theta = 0°$, (b) 45°, and (c) −45°, the normalized results for the S-type (momentum flux) and P-type (particle flux) probes, using the mean value near the measurement point in each experiment as the normalization reference. For $\theta = 0°$, the experimental data and the simulation results for $\alpha = 0.9$ are in good agreement. The simulation also reproduces the observed decrease in flux at the probe position (0°). For $\theta = \pm 45°$, the result with $\alpha = 0.9$ again shows the smallest error, although the discrepancy becomes more pronounced at around $\theta = \pm 25°$. This is likely due to the limitations of the Maxwell reflection model, indicating the potential need to introduce a CLL reflection model, which can reproduce more realistic gas-surface interactions.

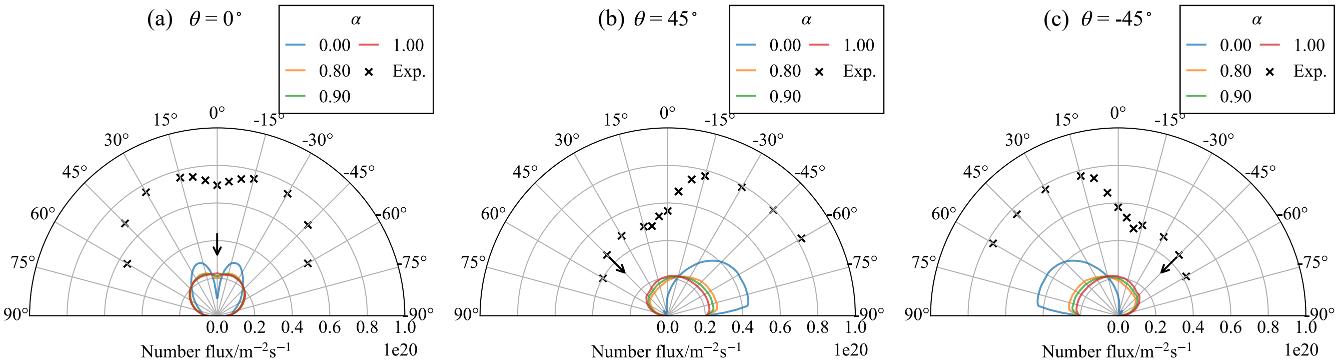

Fig. 9. Simulation results of the particle number flux in the probe radial direction for different values of the accommodation coefficient α with (a) $\theta = 0°$, (b) 45°, and (c) −45°. Cross plots indicate experimental values.[11)]

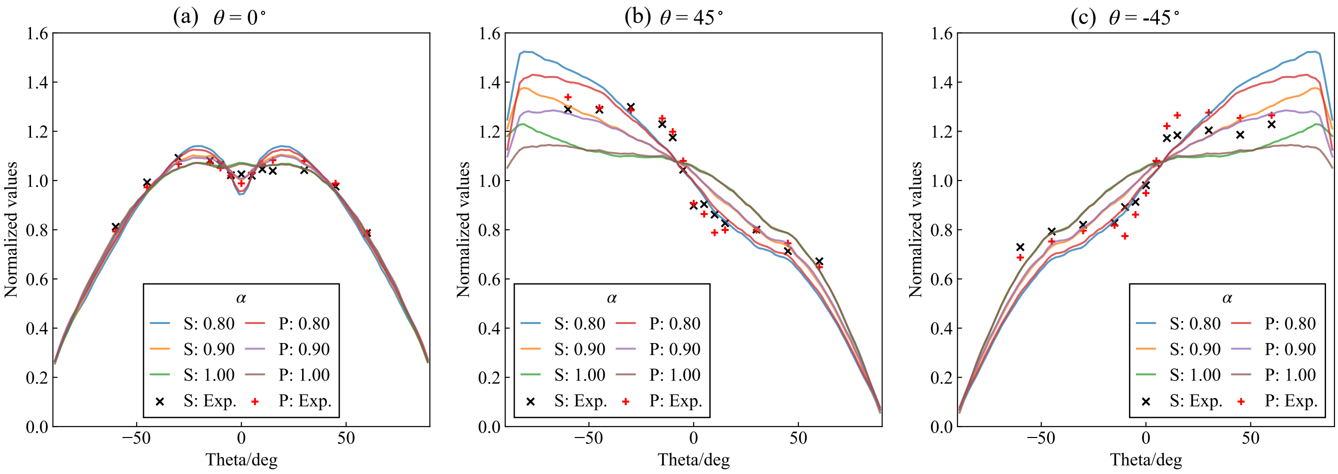

Fig. 10. Normalized values for different values of the accommodation coefficient α with (a) $\theta = 0°$, (b) 45°, and (c) −45°. "S" indicates normalized momentum flux, and "P" indicates normalized particle flux.

4. Conclusion

In this study, we developed a GPU-accelerated DSMC solver with adaptive mesh refinement and applied it to the simulation of rarefied xenon gas flows in a vacuum chamber. The numerical model was constructed to closely replicate recent experimental setups employing S-type and P-type rarefied gas measurement devices. By systematically varying both the wall accommodation coefficient and the gas injection angle, the simulations provided insights into how neutral particle distributions, as well as momentum and particle fluxes, are affected by different surface reflection models.

Quantitative comparison with experimental data showed that the absolute values were not always consistent, mainly due to pressure measurement uncertainties and the use of simplified analysis models. However, when the results were normalized, the simulations reproduced the experimental trends well. Notably, the best agreement was observed for accommodation coefficients around $\alpha = 0.9$. These findings emphasize the importance of accurate modeling of gas-surface interactions. Future work will include introducing a more rigorous reflection model, such as the CLL model, and performing simulations that incorporate the detailed structure of the measurement devices, in order to further improve the accuracy of the analysis.

Acknowledgments

This work was partially supported by the Multidisciplinary Cooperative Research Program in CCS, University of Tsukuba, and by "Joint Usage/Research Center for Interdisciplinary Large-scale Information Infrastructures (JHPCN)" in Japan (Project ID: jh250022).

References

1) Brown, D. L. and Gallimore, A. D., "Evaluation of Facility Effects on Ion Migration in a Hall Thruster Plume," *Journal of Propulsion and Power*, Vol. 27, No. 3, May 2011, pp. 573–585.
2) Foster, J. E. and Topham, T. J., "A review of the impact of ground test-related facility effects on gridded ion thruster operation and performance," *Physics of plasmas*, Vol. 31, No. 3, March 2024.
3) Ito, G., Kawashima, R., Komurasaki, K., and Koizumi, H., "Method of Suppressing Ingestion Particles Flowing Back to a Hall Thruster using a Beam Target during Ground Testing," *Transactions of the Japan Society for Aeronautical and Space Sciences*, Vol. 65, No. 4, 2022, pp. 160–171.
4) Nishii, K. and Levin, D. A., "Three-Dimensional Kinetic Simulations of Carbon Backsputtering in Vacuum Chambers from Ion Thruster Plumes," *Journal of Propulsion and Power*, Vol. 40, No. 1, Jan. 2024, pp. 123–137.
5) Agrawal, A. and Prabhu, S. V., "Survey on measurement of tangential momentum accommodation coefficient," *Journal of vacuum science & technology. A, Vacuum, surfaces, and films: an official journal of the American Vacuum Society*, Vol. 26, No. 4, July 2008, pp. 634–645.
6) Sharipov, F. and Moldover, M. R., "Energy accommodation coefficient extracted from acoustic resonator experiments," *Journal of vac-*

uum science & technology. A, Vacuum, surfaces, and films: an official journal of the American Vacuum Society, Vol. 34, No. 6, Nov. 2016, pp. 061604.

7) Yamaguchi, H., Mori, T., Ozaki, Y., Matsuda, Y., and Niimi, T., "Experimental measurements of thermal and tangential momentum accommodation coefficients on solid surfaces: Water vapor in comparison with noble gases," *International journal of heat and mass transfer*, Vol. 183, No. 122195, Feb. 2022, pp. 122195.
8) Nakayama, Y., "Rarefied propellant flow vector measurement within a vacuum chamber," *TRANSACTIONS OF THE JAPAN SOCIETY FOR AERONAUTICAL AND SPACE SCIENCES AEROSPACE TECHNOLOGY JAPAN*, Vol. 18, No. 5, 2020, pp. 174–179.
9) Nakayama, Y., "Propellant Flow Vector Measurement within a Vacuum Chamber with Three Types of Rarefied Flow Detectors," *Proceedings of the 37th International Electric Propulsion Conference*, 2022.
10) Nakayama, Y., Waseda, S., and Ito, T., "Prototype of a measurement device for evaluating propellant particle reflection phenomena on vacuum chamber walls," *AEROSPACE TECHNOLOGY JAPAN THE JAPAN SOCIETY FOR AERONAUTICAL AND SPACE SCIENCES*, Vol. 23, No. 0, 2024, pp. 49–52, (in Japanese).
11) Kukiyama, H., Oda, M., Ito, T., and Nakayama, Y., "Fundamental Experimental Evaluation of Wall Reflection Phenomenon Measuring Apparatus Using Rarefied Flow Measuring Devices," *Proceedings of the 68th Space Sciences and Technology Conference*, P205, 2024, (in Japanese).
12) Bird, G. A., *Molecular Gas Dynamics and the direct simulation of gas flows*, The Oxford engineering science series, Oxford University PressOxford, May 1994.
13) Nishii, K., "Numerical study of facility pressure effects on micronozzles for space propulsion," *AIAA journal*, Vol. 63, No. 1, Jan. 2025, pp. 344–353.
14) Berger, M. and Colella, P., "Local adaptive mesh refinement for shock hydrodynamics," *Journal of Computational Physics*, Vol. 82, May 1989, pp. 64–84.
15) Korkut, B., Li, Z., and Levin, D. A., "3-D Simulation of Ion Thruster Plumes Using Octree Adaptive Mesh Refinement," *IEEE transactions on plasma science. IEEE Nuclear and Plasma Sciences Society*, Vol. 43, No. 5, May 2015, pp. 1706–1721.
16) Martin, R. S. and Cambier, J.-L., "Octree particle management for DSMC and PIC simulations," *Journal of computational physics*, Vol. 327, No. C, Dec. 2016, pp. 943–966.
17) Nakayama, Y., "Rarefied dynamic pressure vector measurement of electric propulsion propellant flows," *Journal of the Japan Society for Aeronautical and Space Sciences*, Vol. 65, No. 5, 2017, pp. 200–207, (in Japanese).